Pursuing the Spatial Organization of Lineage-Determining Genes of Hematopoiesis

Jinming Liu

A thesis
submitted in partial fulfillment of the
requirements for the degree of

Master of Science in Applied Chemical Science and Technology

University of Washington
2026

Committee:
Dr. Joshua C. Vaughan
Dr. Dan Fu

Program Authorized to Offer Degree:

Chemistry

University of Washington

Abstract

Pursuing the Spatial Organization of Lineage-Determining Genes of Hematopoiesis

Jinming Liu

Chair of the Supervisory Committee:
Dr. Joshua C. Vaughan
Departments of Chemistry and Physiology & Biophysics

Hematopoiesis is the continuous, highly regulated process, during which all mature blood cell types are generated from a small pool of hematopoietic stem cells (HSCs). The commitment of HSCs and multipotent progenitors to specific lineages, namely, myeloid, erythroid, and lymphoid, is governed by a network of lineage-determining transcription factors, including PU.1 (encoded by *Spi1)*, GATA-1 (encoded by *Gata1)*, and TCF1 (encoded by *Tcf7*). The activities of these transcription factors and their roles in hematopoietic cell differentiation are closely related to the epigenetic states of the chromatin at their gene loci. While sequencing methods such as ChIP-seq and CUT&RUN have established the genome-wide distribution of histone modifications in blood cells, these approaches are inherently limited by their inability to resolve cell-to-cell variation or to provide spatial information at the single-cell level.

This thesis applies a recently developed method, Single Cell Evaluation of Post-TRanslational Epigenetic Encoding (SCEPTRE), to murine hematopoietic cells. SCEPTRE

integrates Expansion Microscopy (ExM), DNA fluorescence in situ hybridization (FISH), and immunofluorescence to simultaneously visualize histone modifications and specific gene loci in intact single cells. The first goal of this thesis was to validate ExM and DNA FISH as robust and reproducible methods for studying murine bone marrow derived macrophages (BMDMs), as SCEPTRE had not previously been applied to this primary cell type. The second goal was to begin the characterization of the spatial distribution of histone modifications and chromatin structures relative to the three lineage-defining gene loci: *Spi1*, *Gata1*, and *Tcf7*.

Acknowledgements

I'm deeply grateful to Professor Joshua Vaughan, without whose patience and guidance, nothing from this work would have been possible. Josh is funny, understanding, supportive, and often shares fun anecdotes, yummy cookies, and chocolates during group meetings that make grad school ever so slightly more enjoyable. I also owe many thanks to Dr. Madeline Wong, who took me under her supervision two years ago and has since endured my many foolish questions like how to cut open a mouse, or what immunostaining meant. I also want to thank everyone else in the Vaughan Group: Chris Kim, Hannah Perry, Yuka Kurasaka, Pedro Vasquez, Wenhui Xie, Erica Peterson, Trevor Odell, Eunjin Jo, Yvonne Guan, and Ziyu Guo, many of whom have become dear friends to me. In particular, I want to thank Chris and Pedro for their company on many hikes, trips to the ski slopes, and many board game days.

Outside of the members of the Vaughan Group, I would also like to thank Jimin and Vardhan for their friendships, especially during the first year of my master's program.

Lastly, I would like to thank my parents, for their unconditional support for every decision I've made.

Table of Contents

List of Figures

Chapter 1

Chapter 2

List of Tables

Chapter 2

Chapter 1 Introduction

1.1 Hematopoiesis

Hematopoiesis, the continuous process of blood cell generation throughout an organism's lifetime, is essential to the lives of all vertebrates.[1–3] It is a highly complex, yet highly regulated process, controlled by the hematopoietic system and takes place primarily in the bone marrow for adults. The hematopoietic system is often viewed as a hierarchy, where the hematopoietic stem cells (HSCs) sit at the apex, characterized by their self-renewal abilities and pluripotency (Fig.1). As HSCs progressively differentiate into multipotent progenitors, and then into lineage-specific, unipotent progenitors, they also lose their self-renewal abilities.[4] Eventually, the progenitors differentiate into specialized cells, such as red blood cells, macrophages, platelets, and T cells, among others.[5] There are three main lineages in the hematopoietic system: erythroid, myeloid, and lymphoid. Erythroid differentiation of HSPCs (hematopoietic stem and progenitor cells) produces blood components such as red blood cells and platelets; myeloid differentiation primarily produces innate immune cells, including granulocytes and macrophages; and lymphoid differentiation results in innate and adaptive immune cell types, including T-cells, B-cells, and natural killer cells.[6,7] Matured blood cells have relatively short life spans (e.g. only several days for granulocytes), so they must be continuously replenished in large numbers.[6,8] For example, a healthy adult human produces approximately 4-5 x 10^{11} mature blood cells every day, and for a healthy mouse, approximately 0.5-1.5 x 10^{9} per day.[9]

A balanced regulation of the hematopoietic system requires a large quantity but also with a high specificity. The accumulation or deprivation of any cell type can be problematic. For example, a reduction in the production of red blood cells causes anemia, an accumulation of undifferentiated myeloid precursors in the bone marrow leads to acute myeloid leukemia, and a disruption in the production of lymphocytes leads to lymphopenia, which can lead to further

autoimmune conditions.[10–12] The various diseases that can be caused by an improperly regulated hematopoietic system underline the importance of the strict control of cell fate determination, and a better understanding of the underlying mechanisms can have substantial clinical relevance, such as in the case of differentiation therapy.[13]

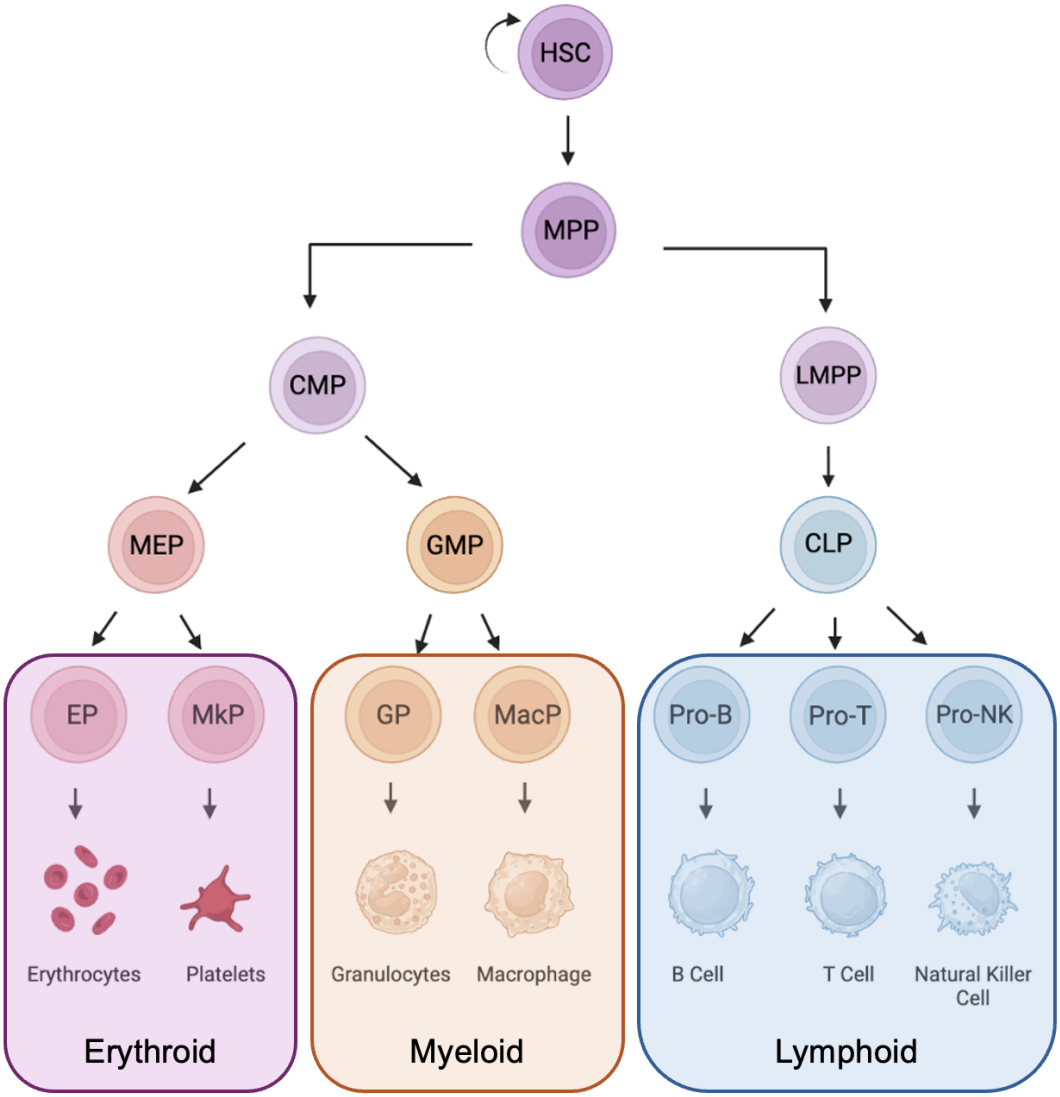

Figure 1. Schematic of the hierarchy of the hematopoietic system. At the top are HSCs, that are pluripotent, self-renewal, and can differentiate into all the mature blood cell types. The next stage includes multipotent progenitors: CLP, common lymphoid progenitors, and CMP, common myeloid progenitors. The next stage below is committed progenitors which differentiate into

only one lineage. The last stage is when cells reach their final specialized and mature cell type. Created with BioRender.com.

1.2 Chromatin organization as a determinant of gene expression

Gene expression is regulated at multiple scales. The macroscale considers the territories individual chromosomes occupy within the nucleus. The intermediate, mesoscale, considers the topologically associating domains (TADs) that facilitates enhancer-promoter communications. The microscale considers the histone post-translational modifications (PTMs), and nucleosome positioning, and the accessibility of DNA sequences.[14] The nucleosome (Fig.2), composed of approximately 147 base pairs of DNA wrapped around an octamer of 4 histone protein pairs (H2A, H2B, H3, and H4), is the fundamental repeating unit of chromatin. Linker histone H1 binds intervening DNA between adjacent nucleosomes, also contributing to higher-order chromatin folding and compaction. This arrangement allows the nearly two meters of genomic DNA to fit within the confined space of the nucleus while still remaining accessible for regulated gene expression.[15–17]

There are approximately 2.7 billion base pairs (Gbp) in the mouse genome, in any given cell type, a large fraction of the genes is transcriptionally silent or repressed. Consequently, though all nucleated cells in an organism contain essentially the same DNA content, different cell types and functions exist because of their differences in gene expression.[17–19] As mentioned in Chapter 1.1, HSCs are characterized by their self-renewal abilities and pluripotency, and as they differentiate into specialized cells, the genes associated with self-renewal are silenced and cell-type specific genes are activated. There are regulatory elements that are sequences found on the DNA, such as promoters, enhancers, silencers, and insulators, that encode intricate programs

that control cellular functions. For example, they can recruit transcription factors (TFs) that control transcription initiation, the rate of chromatin compaction, and the release of RNA polymerase II.[20] However, gene expression is multi-faceted, and additional regulatory information associated with cell differentiation exists beyond simply the DNA sequences.[21]

Without changing the fundamental DNA sequences, epigenomic modifications such as DNA methylation and post-translational modifications (PTMs) to histone proteins (histone marks) also play a huge role in gene expression. The histone core is predominantly globular with the exception of their unstructured N-terminal "tails", which allows for a large number and different types of modifications, including methylation, acetylation, phosphorylation, ubiquitination, and more. These modifications can alter the higher-level chromatin structures through two mechanisms: by recruiting nonhistone proteins with specific enzymatic activities that lead to chromatin-remodeling, or by directly disrupting the interactions between nucleosomes.[22,23]

By changing the compaction of the chromatin structures, PTMs change DNA accessibility and control gene expression. Generally, the accessibility of chromatin is seen to be on a spectrum with two extremes (Fig.2). The most accessible form of chromatin is in an expanded, "open," state and transcriptionally active, commonly known as "euchromatin"; the most compact, "closed," and transcriptionally inactive form is commonly referred to as "heterochromatin." Heterochromatin can be further categorized into constitutive heterochromatin, which are more stable and contains repetitive DNA elements, and facultative heterochromatin, which are more dynamic in comparison.[24,25] Histone acetylation generally reduces chromatin compaction which promotes transcriptional activation, whereas histone deacetylation promotes compaction and represses transcriptional activities. Histone methylation

is more context-dependent, with modifications such as H3K4me3 associated with activation, and H3K27me3 associated with repression, both of which will be further discussed in Chapter 1.3. The chromatin states can impact cellular activities like DNA replication, DNA repair, and cell division. Importantly, chromatin organization is not static, and the actual spatial and temporal organization of chromatin is continuously changing in response to developmental and environmental cues.[24,27]

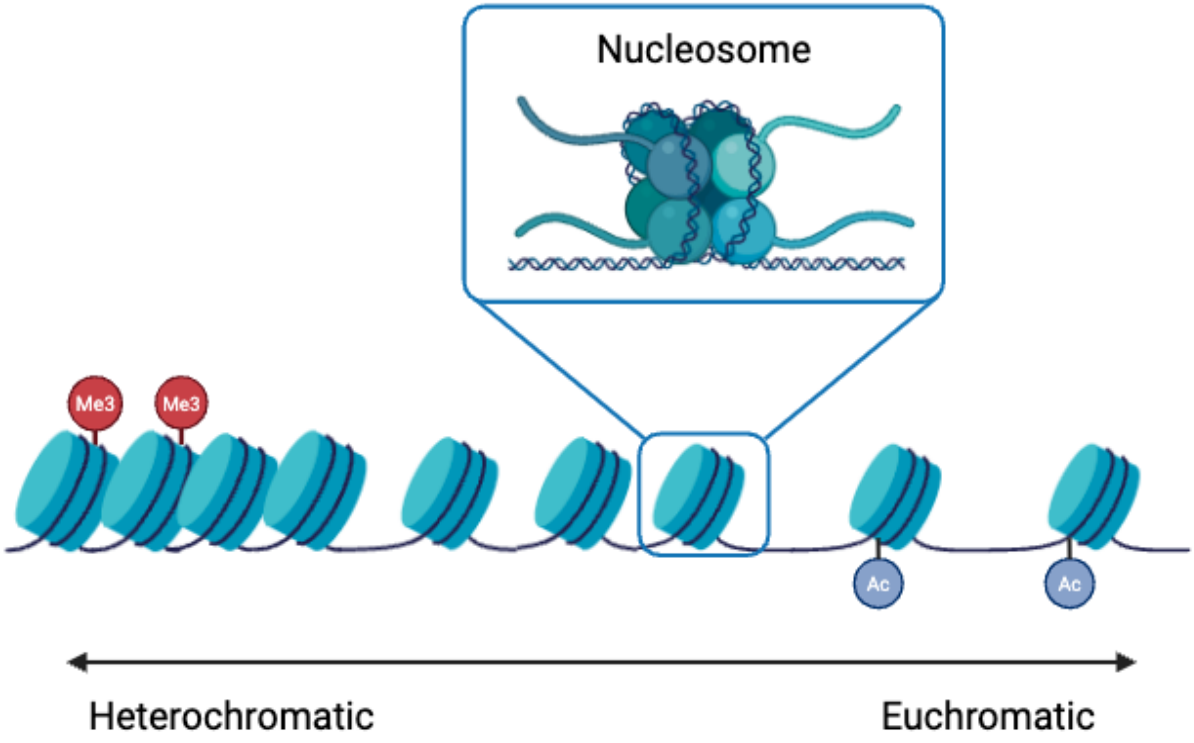

Figure 2. Chromatin organization. The individual repeating units of chromatin are nucleosomes, which contain 147 bp wrapped around four pairs of histone proteins. The histone tails are subject to post-translational modifications, which result in different levels of compaction of the chromatin structure. Heterochromatin is more compact, less transcriptionally active. Euchromatin is more relaxed, more transcriptionally active. Created with BioRender.com.

1.3 The bivalency of H3K27me3 and H3K4me3

In cell development, as pluripotent stem cells transition into more specialized cell types, they lose their pluripotency and acquire stable lineage-specific gene expressions. This transition does not involve changes in DNA sequence but is mediated by chromatin modifications, many of which are reversible. A key feature of early developmental potential is bivalency. Bivalency is a common occurrence in embryonic stem cells, where both activating (e.g. H3K4me3) and repressive (e.g. H3K27me3) marks are present at the same site. These marks are maintained by opposing enzymatic complexes; Trithorax group regulates H3K4me3 and promotes gene activation, while Polycomb complexes deposit H3K27me3 and enforces gene repression.[28,29] The balance between the two complexes creates an intermediate state that allows genes to respond to developmental and environmental cues, where the genes can be repressed by losing the H3K4me3 modification, or become activated by losing the H3K27me3 modification. These changes are directed by lineage-defining transcription factors that recruiting chromatin-modifying enzymes, such as histone acetyltransferases and histone deacetylases, to initiate chromatin changes near the binding sites, enabling precise control over gene expression as cells commit to particular fates.[25,30]

1.4 Lineage-defining genes in the hematopoietic system

To study the spatial distribution of lineage-defining genes in relation to chromatin structures and histone marks, we chose *SPI1*, *GATA1*, and *Tcf7*, representing the myeloid, erythroid, and lymphoid lineages, respectively.

PU.1, encoded by the *SPI1* gene, is a key transcription factor that regulates at least 3,000 genes expressed in hematopoietic cells and functions in a dosage-dependent manner. It is central to cellular specification from pluripotent progenitor cells, particularly in regulating the balance

between lymphoid and myeloid development.[13] PU.1 functions as a non-classical pioneer transcription factor, meaning it can enhance chromatin accessibility by recruiting remodeling complexes (e.g., the SWI/SNF complex), though it lacks the ability to access target sites in the nucleosome itself.[31,32] In hematopoietic progenitors, PU.1 is expressed at an intermediate level, but during differentiation, a higher PU.1 level favors myeloid differentiation, and a lower level of PU.1 generally leads to lymphoid development. The expression levels of PU.1 is self-regulated by positive feedback loops: high PU.1 levels in macrophages promote cell cycle lengthening, which in turn allows the stable maintenance of high PU.1 expression.[33]

GATA-1 is a zinc-finger transcription factor central to the differentiation of erythroid and megakaryocytes but prevents the development of granulocyte-monocyte and lymphoid. A high level of GATA-1 expression is also observed in differentiated mast cells and eosinophils. GATA-1 does not act alone; its interactions with the Friend of GATA-1 (FOG-1) family is required in many GATA factor activities, including in erythroid and megakaryocyte development.[34,35] GATA-1 and PU.1 engage in mutual antagonism, either transcriptionally or through direct protein-protein interactions, such that PU.1-dominant progenitors are pushed toward granulocyte, monocyte, and lymphoid fates, while GATA-1-dominant progenitors are directed toward erythroid.[13] There is likely a stoichiometric relationship between PU.1 and GATA-1 that determines the gene expression associated with each lineage outcome. Despite their mutual repression in the aforementioned specifications, however, PU.1 and GATA also work together to promote the differentiation of eosinophil and mast cells. Mutations in GATA-1 that result in a truncated protein lacking certain functional sites are associated with various hematologic disorders, such as acute megakaryoblastic leukemia and transient abnormal myelopoiesis in children with Down syndrome.[13,36]

T cell factor 1 (TCF1), encoded by *Tcf7*, is the earliest T cell specific transcription factor and acts as a lineage-determining factor that establishes the epigenetic identity of T cells. It is upregulated in early thymic progenitors in direct response to Notch1 signaling and is sustained through maturation.[3] TCF1 acts upstream of several T cell identity genes, such as *Gata3*, *Il2ra*, and *Bcl11b*.[37] In *Tcf-7* deficient mice, T lineage-like cells do not have the same level of chromatin accessibility like normal T cells and are functionally limited, in terms of differentiation and persistence during infection. Additionally, TCF1 possesses intrinsic histone deacetylase (HDAC) activity, which establishes and maintains the dichotomy between $CD4^+$ and $CD8^+$ T cells, by repressing $CD4^+$ T lineage-associated genes in CD8+ T cells.[38] It targets silent chromatin regions, and some TCF1 binding events are associated with gaining active enhancer mark H3K27ac or losing repressive marks H3K27me3 and H3K9me3. Together, these transcriptional and chromatin remodeling functions directly link TCF1 to the epigenetic control of T cell identity.[37,39]

1.5 Methodologies for histone mark detection: sequencing-based methods vs SCEPTRE

There are several popular and well-established techniques that can be used to map the epigenome and measure chromatin accessibility, such as chromatin immunoprecipitation sequencing (ChIP-seq) or CUT&RUN.[40,41] ChIP-seq is a powerful tool used for mapping histone modifications and transcription factor binding sites in a genome-wide manner at base-pair resolution. ChIP-seq has many advantages, including high resolution, low noise, and broad genome coverage.[42] CUT&RUN is another high-throughput epigenomic profiling method, which maps protein-DNA interactions with the cells and nuclei staying intact. It has an even higher signal-to-noise ratio than ChIP-seq and is free of DNA accessibility artifacts.[43] However, sequencing based approaches are limited to studying one histone modification at a time,

generally in large ensembles, and are not able to capture cell to cell variations within a population. To visualize and quantify multiple histone modifications on a single cell level, Vaughan and Kueh labs developed a method called Single Cell Evaluation of Post-TRanslational Epigenetic Encoding (SCEPTRE), which was utilized for the research of this thesis.[44]

SCEPTRE integrates three established techniques: Expansion Microscopy (ExM), DNA fluorescence in situ hybridization (FISH) and immunofluorescence to visualize and quantify histone mark signals in relation to individual gene loci. ExM is a technique that physically expands the sample of interest, 4-to 20-fold, on a swellable gel, which allows the examination of the cell features that are below the light diffraction limit. Conventional fluorescence microscopy is diffraction-limited to a resolution of roughly 200-300 nm, whereas 4x expansion brings the effective resolution to approximately 60 - 70 nm with a conventional microscope.[44,45] FISH is a widely used and versatile technique that incorporates fluorophores to allow the visualization of nucleic acid sequences under a microscope, and immunofluorescence staining is used in parallel to visualize the distribution of histone modifications. Combining immunofluorescence with DNA FISH is typically challenging, because the harsh denaturing conditions required for DNA FISH can remove antibody labels prior to FISH. ExM overcomes the challenge by covalently anchoring immunostained labels to the hydrogel before expansion, preserving the signals through subsequent FISH steps.[44] A bisbenzimide dye, Hoechst 33258, is used in parallel to label A-T rich DNA regions to visualize the overall chromatin structures.[46] Together, these techniques enable simultaneous and high-resolution imaging of gene loci, histone modifications, and chromatin structures within intact single cells.

ExM is a well-established method for studying tissue and cultured cells, but physical differences exist between specimens, so imaging registration of before and after expansion of the

same blood cells is important for validation. Comparing and aligning the before and after images of the same samples allows a distortion analysis to assess the quality of the expansion, and if optimization of the procedures is necessary. Image registration of before and after DNA FISH is also necessary to assess if the harsh hybridization conditions introduce artifacts or cause large distortions that could compromise spatial measurements (Figure 3b).

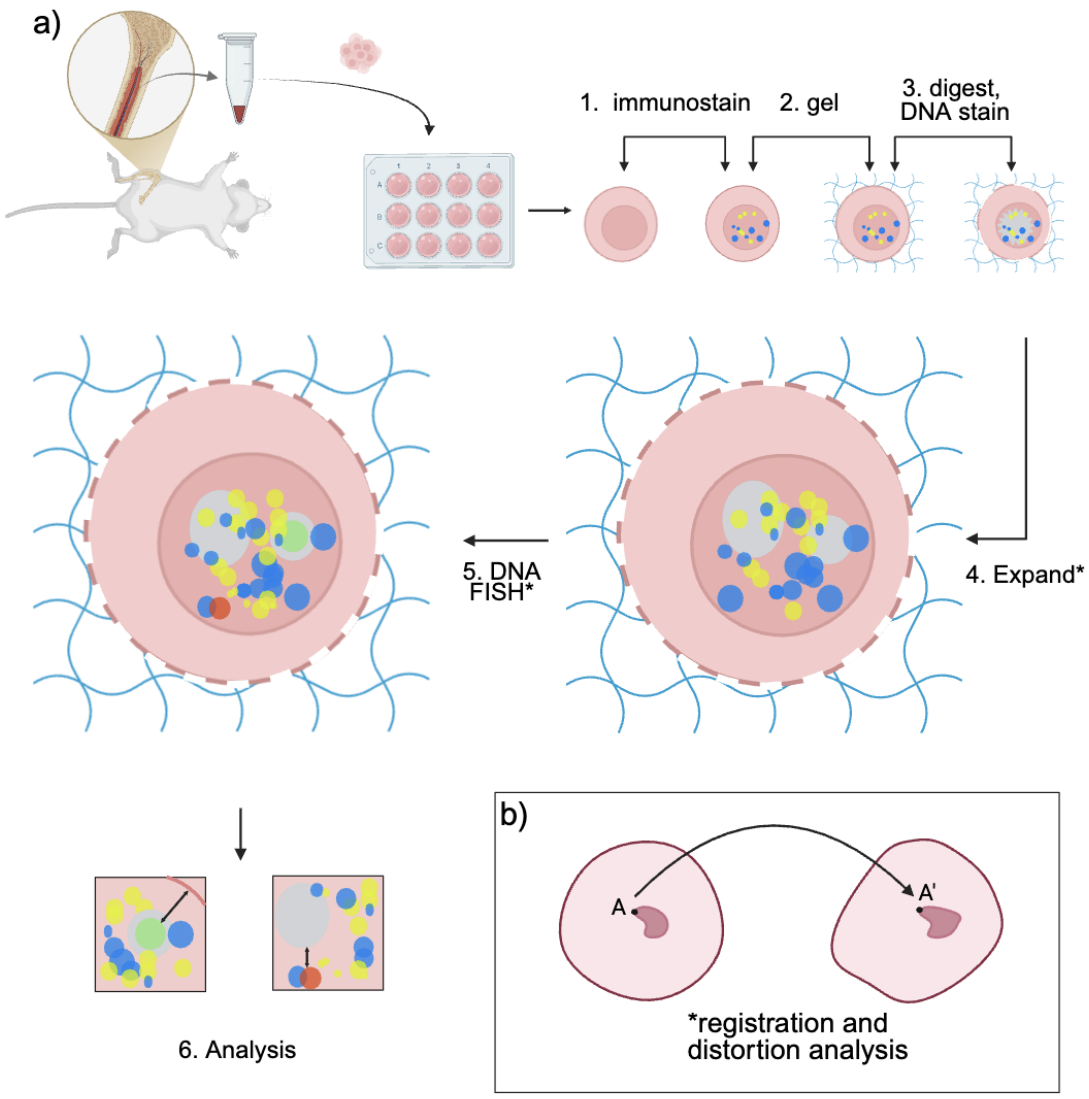

Figure 3. Overall workflow. a) 1) Immunostaining of histones. 2) Gelation, where sample and antibodies become linked to the hydrogel. 3) Digestion with proteinase K and Hoechst 33528 staining. 4) Expansion of sample, ~ 4x. A pre-post expansion registration and distortion analysis was performed. 5) DNA FISH. A pre-post DNA FISH registration and distortion analysis was performed. 6) Measured distance from gene loci to chromatin structures and nuclear edge. b) Schematic of image registration.

1.6 Summary

This thesis aims to achieve two goals: first, to validate ExM and DNA FISH as robust methods for studying murine BMDMs, and second, to begin the characterization of the spatial distribution of histone modifications and chromatin structures relative to three gene loci, namely, *Spi1*, *Gata1*, and *Tcf7* in macrophages. Using SCEPTRE to achieve these goals enables single cell quantification of histone modification levels and allows observation of cell-to-cell variations that bulk sequencing methods cannot capture.

Chapter 2 Method Validation for the Spatial Distribution of Gene Loci

2.1 Introduction

Super-resolution fluorescence microscopy techniques have been utilized to visualize the spatial organization of gene loci, histone marks, and nucleosomal clusters within individual cells. However, most studies were limited to viewing gene and histone marks separately due to the challenge of combining DNA FISH and immunofluorescence. To overcome this challenge, the Vaughan and Kueh labs have developed Single Cell Evaluation of Post-TRanslational Epigenetic Encoding (SCEPTRE) that allows the combination of the two methods by incorporating expansion microscopy (ExM). [44] By covalently anchoring the antibodies and proteins on a swellable gel, ExM is able to preserve the signals from immunofluorescence in the harsh environment (e.g. high denaturation temperature and high formamide concentration) during DNA FISH. Together, SCEPTRE allows the concurrent visualization and quantification of multiple histone modifications at non-repetitive gene loci in single cells.

SCEPTRE has been established to work well with lab-derived cell lines such as h-TERT RPE1 cells, but it has not been used on mouse-derived primary cells. Additionally, despite ExM's wide applications in different tissues and cultured cells, the expansion quality is dependent on sample properties, and there are still possibilities of distortion due to over-crosslinking of proteins, low mechanical stability of the hydrogel, or incomplete sample homogenization. [47,48] Because pre-post ExM distortion analysis has never been performed on BMDMs, it is necessary to validate that expansion does not distort BMDMs. The stringent denaturation conditions of DNA FISH could introduce additional structural distortions beyond those from expansion, so a pre-post DNA FISH comparison is also necessary to assess the amount of distortion that might arise from FISH.

2.2 Results for pre-post analyses

2.2.1 Pre-expansion vs post-expansion distortion analysis

To simplify the process of locating the same cells before and after expansion, after fixing the cells, but before gelation and expansion, the bottom of the 8-well chamber slide was marked with a permanent marker before pre-expansion image acquisition. After gelation, and before expansion, the top right of the gel was cut off to aid orienting the gel correctly after expansion.

Pre-expansion images were acquired using a 20x objective to create a reference grid with dimensions of approximately ~ 665 μm x 3300 μm. An easily identifiable cluster was selected and was imaged with a 60x objective. A cluster of Hoechst 33258-stained BMDM nuclei were imaged pre-expansion, and the corresponding post-expansion images of the same nuclei were subsequently acquired. All images for pre-post comparison purposes were obtained on a 60x 1.27 NA water-immersion objective on a homebuilt spinning disk confocal microscope. After image acquisition, each sample was cropped, processed, and analyzed using open-source software packages in imageJ, *Elastix*, and *Python.*

Image registration was performed using *Elastix,* over a two-step process: an initial rigid (similarity) transformation (Fig. 1b) to correct for global translation, rotation, and magnification, followed by a non-rigid (B-spline) transformation (Fig. 1g) to capture local deformation. The post-expansion image after similarity transformation was compared to the pre-expansion image, and there was visually little distortion (Fig 1b-f). To quantify the distortion, points that were the same distances apart in the pre-expansion image were grouped together, and the root mean square error of each group was calculated based on how much the distances between the same points changed in the post-expansion image, and plotted against the true distance (Fig. 1h and i).

The overall distortions were very small, less than 0.2 µm over a typical macrophage nucleus of ~10 µm.

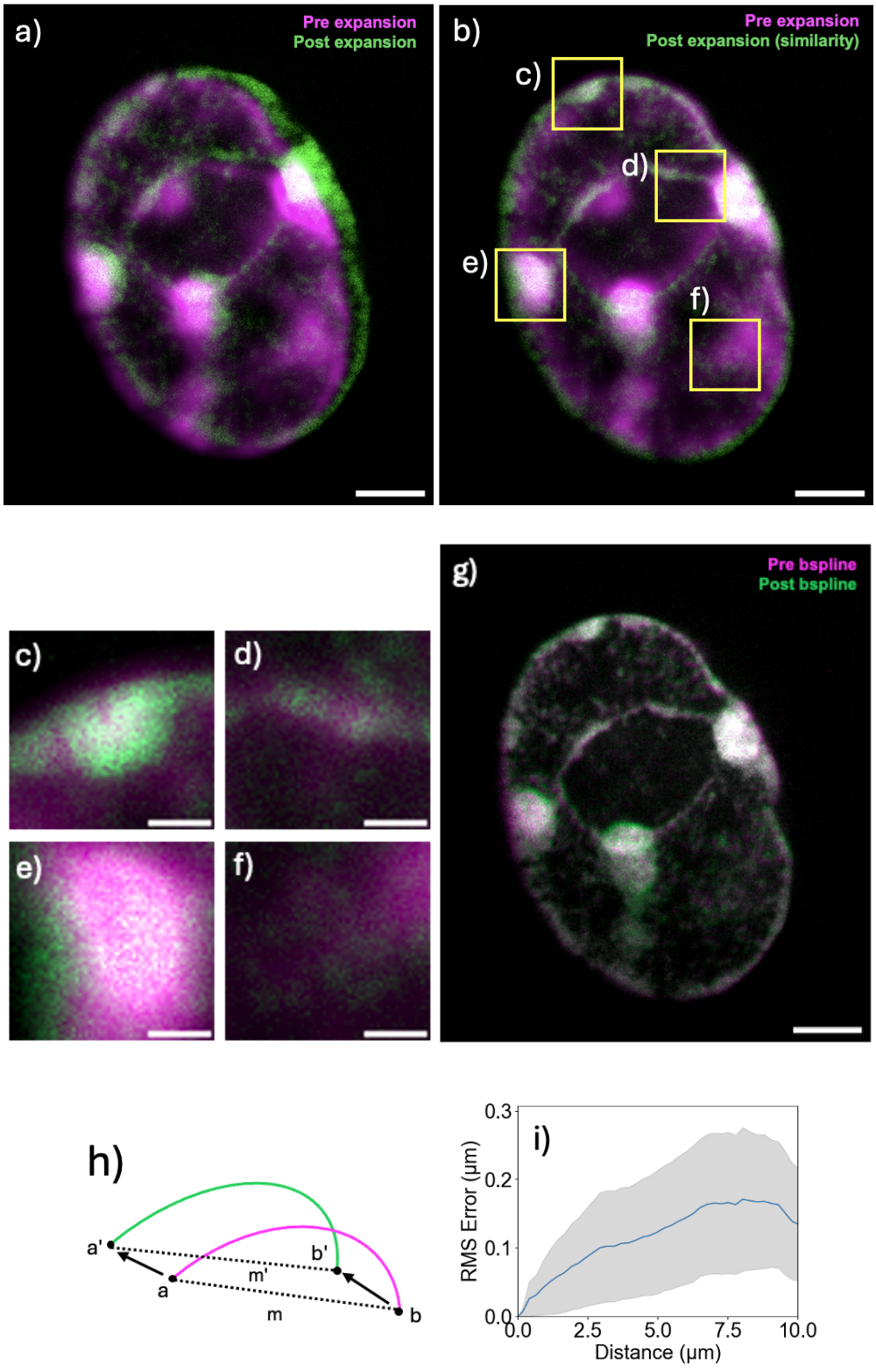

Figure 1. Comparison of pre-expansion and post-expansion images of a murine BMDM nucleus, stained with Hoechst 33258, captured by confocal fluorescence microscopy. a) Overlay of the same macrophage nucleus pre (magenta) and post (green) expansion, where the pre-expansion image was scaled 4.3x using ImageJ. b) Overlay of the same macrophage nucleus pre-expansion (magenta) vs post-expansion after similarity registration (green). c) Overlay of the post expansion macrophage nucleus pre (magenta) and post (green) b-spline registration, where the image was locally "warped" so the post-expansion image would better fit the pre-expansion image. d-g) Zoom-in images of c) to show the distortion is relatively small. h) Schematic of how RMS error is calculated. i) Plot of RMS error against the distance between any two points in the original macrophage nucleus. All distances and scale bars shown are pre-expansion cell dimensions. Scale bars a, b, g) 2 μm, c-f) 500 nm.

2.2.2 Pre-DNA FISH vs post-DNA FISH distortion analysis

After gelation and expansion, a portion of the expanded gel with dimensions ~ 5 mm × 10 mm was cut out. To better locate the same cells before and after DNA FISH, the top right corner of the gelled sample was cut off to help with correctly orienting the gel post-DNA FISH. Similar to the process of obtaining pre-expansion images, the pre-DNA-FISH samples were stained with SYBR GREEN I, and an area of the gel with dimensions of approximately ~ 665 μm x 3300 μm was imaged using a 20x objective to create a grid that would assist the identification of the same cells post DNA FISH. An easily identifiable cluster of cells were selected and imaged with a 60x objective. These samples were saved as the pre-DNA FISH samples. After DNA FISH, the same cells were located and imaged again with a 60x objective.

A similar image registration process was performed on the before and after DNA FISH images: a rigid transformation followed by a non-rigid transformation. Though some SYBR

GREEN I signals were lost during the DNA FISH process, the general features and overall shape of the nucleus remained the same in the post-DNA FISH (Fig. 2b) image compared to the pre-DNA FISH image (Fig. 2a). To quantify the distortion, the rms error was again calculated and plotted against the true distance (Fig. 2d).

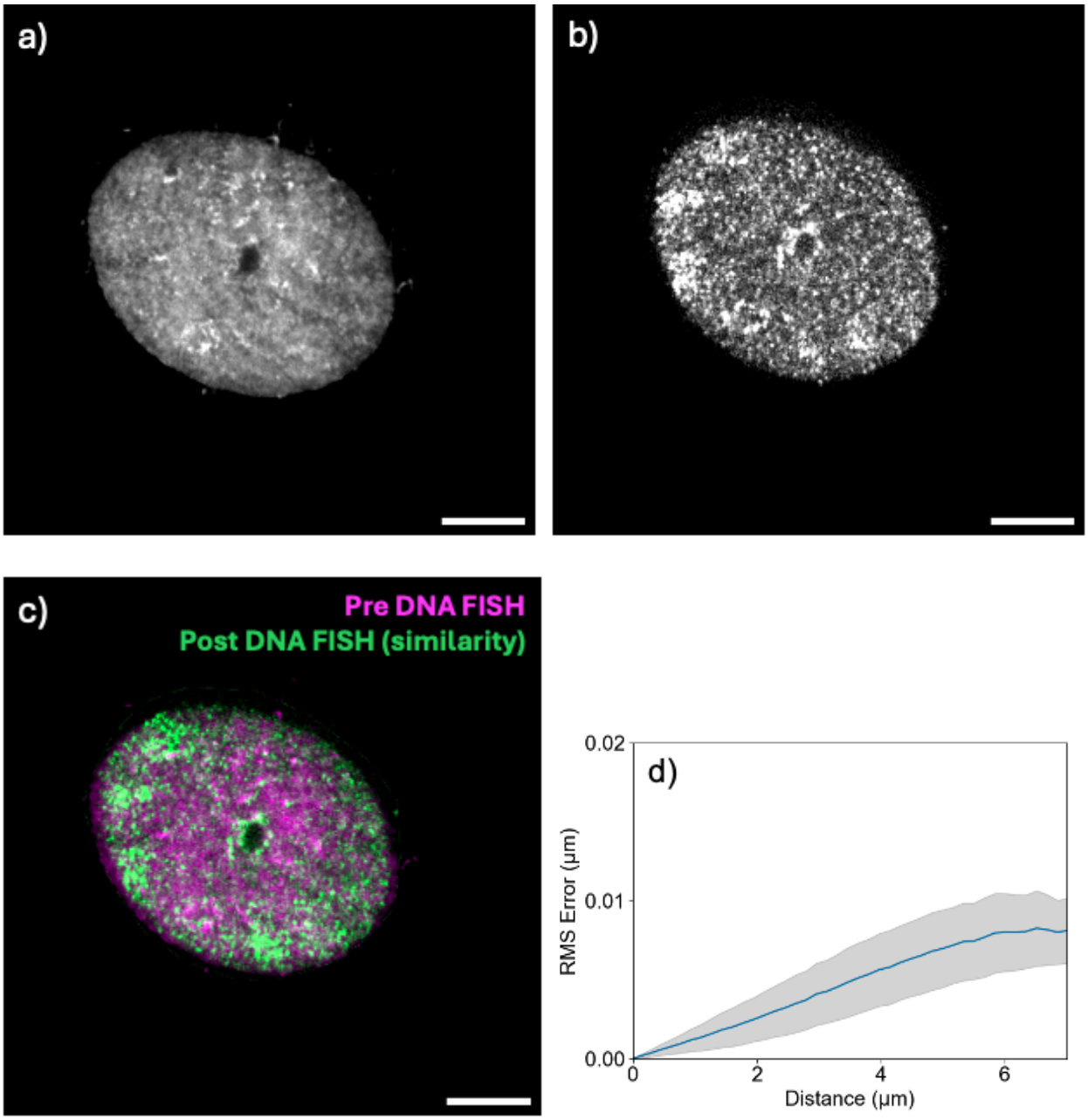

Figure 2. Comparison of pre-DNA FISH and post-DNA FISH images of a murine bone marrow derived macrophage nucleus, stained with SYBR GREEN I, captured by confocal fluorescence microscopy. a) Pre-DNA-FISH image. b) Post-DNA-FISH image. c) Pre DNA FISH shown in magenta, overlaid with post-DNA-FISH image after similarity transform in green. d) RMS error plot. All distances and scale bars shown are pre-expansion cell dimensions. Scale bar: 2μm.

2.2.3 Trouble shooting pre-post DNA FISH

During the experiments, it was observed that the Hoechst 33258 signals were significantly diminished in the post-FISH samples (Fig. 4a-c). Even with an additional staining after FISH, the signals remained dim. Therefore, Alternative DNA stains were tested. The alternative DNA stain TO-PRO-3 (not shown) also photobleached quickly, and the signals became too faint for imaging. A third DNA stain, SYBR GREEN I (Fig. 4), offered the best results and was chosen for the pre-post-DNA FISH distortion analysis.

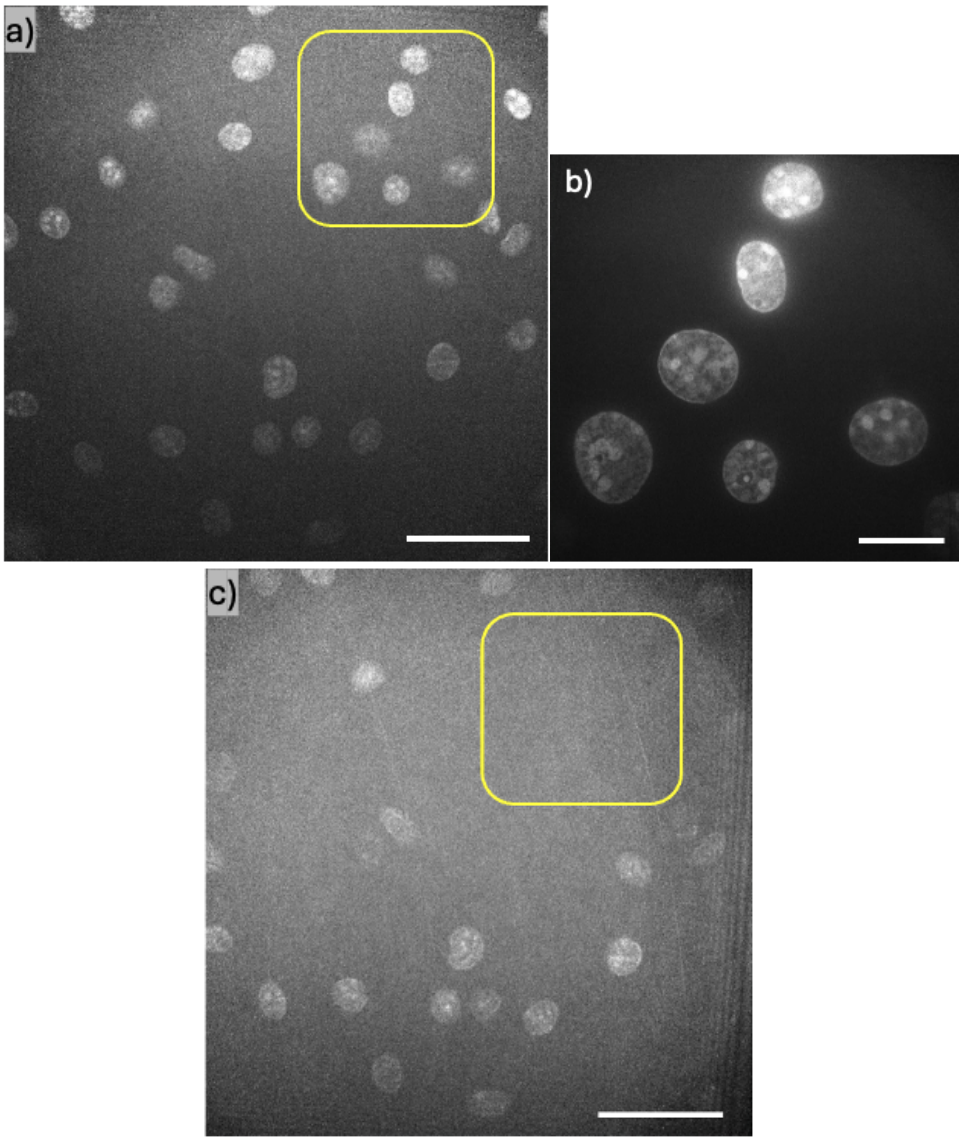

Figure 3. Comparison of pre-and-post-DNA FISH images, stained with Hoechst 33258. a) Pre DNA FISH captured with 60x. b) Pre DNA FISH captured with 20x. c) Post DNA FISH image, captured with 60x. All distances and scale bars shown are pre-expansion cell dimensions. Scale bar: a, c) 50 µm, b) 20µm.

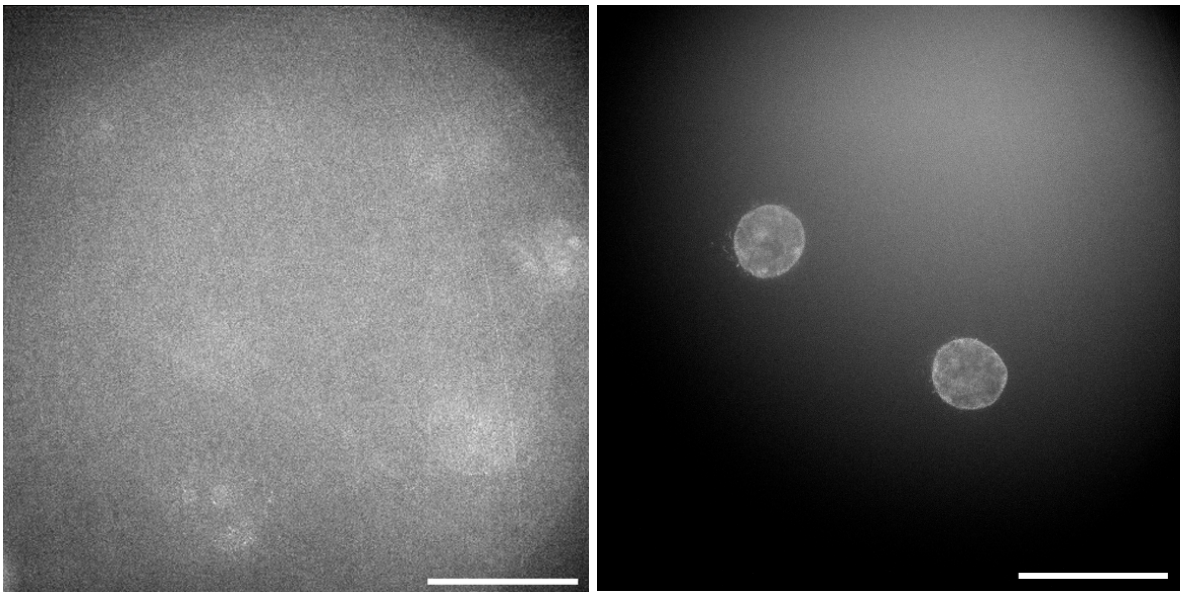

Figure 4. Comparison of post-DNA FISH images stained with Hoechst 3325 and with SYBR GREEN I. Hoechst 33258 (left), SYBR GREEN I (right). The TO-PRO-3 signals photobleached very quickly and became even fainter than Hoechst-33258-stained cells and is therefore not shown. All distances and scale bars shown are pre-expansion cell dimensions. Scale bar: 50 μm.

2.3 DNA FISH data for *spi1*, *gata1*, and *tcf7*

2.3.1 Labeling efficiency

DNA FISH probes targeting *Spi1, Gata1, and Tcf7* gene loci were designed using OligoMiner and applied to BMDMs following the validation process. The labeling efficiency for each gene loci was calculated as the number of cells with at least one gene locus labeled divided by the total number of cells in the sample.

	Spi1	*Gata1*	*Tcf7*
Concentration	600 nM	1200 nM	1200nM
Labeling Efficiency	~90%	~83%	~83%

Table 1. Labeling efficiencies of the *Spi1, Gata1, and Tcf7* FISH probes.

2.3.2 Distance measurements of gene loci to the nuclear periphery

The two-dimensional distance from each detected gene locus to the nearest nuclear periphery was measured in individual cells. To account for inter-cellular differences in nuclear size, the distance from gene loci to the nuclear periphery was divided by the length of the nucleus, measured as the longest diameter of the center slice of the nucleus.

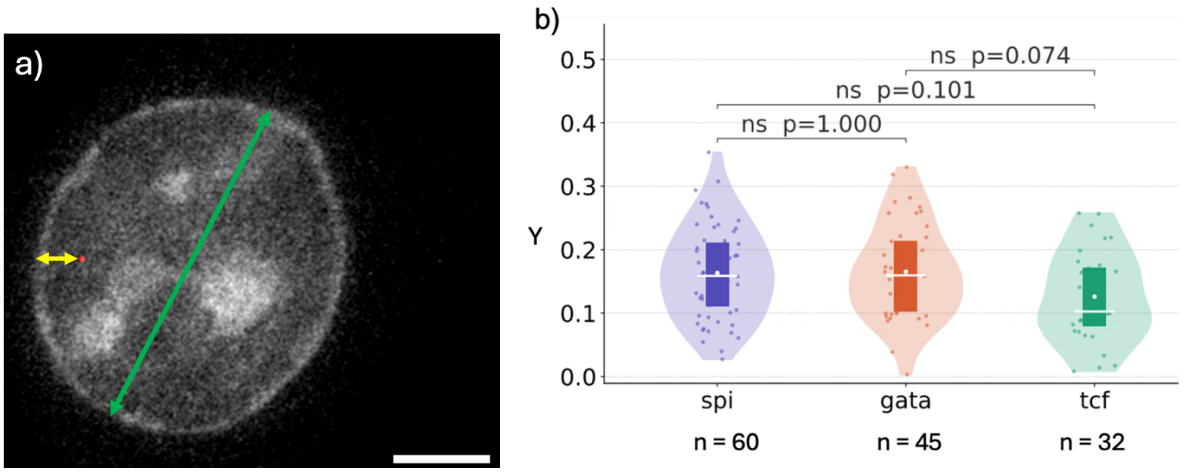

Figure 5. Distance measurement from gene loci to nuclear periphery. a) The shortest distance from the gene locus to the nuclear periphery was measured (yellow) and divided by the length of the nucleus (green). b) A violin plot of the data points measured using the method described in a), where Y axis is the distance from locus to nuclear periphery/length of nucleus, the line is the average, dot the median, and the vertical bar the interquartile range.

Analysis of the resulting distance distribution revealed a general tendency for *Spi1* loci to occupy positions further away from the nuclear periphery relative to *Gata1* and *Tcf7* loci in BMDMs, consistent with the expectation that an actively transcribed myeloid-lineage gene would be positioned away from the transcriptionally repressed nuclear edge. However, the

differences were not statistically significant across the sample sizes studied, due to the substantial cell-to-cell variation. These findings suggest that while a spatial trend may exist, larger sample sizes and/or complementary measurements are required to robustly establish the relationships between *Spi1, Gata1,* and *Tcf7* loci positioning.

2.4 Future directions

2.4.1 Dual-channel DNA FISH

The high cell-to-cell variability in gene loci positioning measurements prompted the development of a dual-channel DNA FISH approach, where *Spi1* and *Gata1* loci are simultaneously labeled within the same cell (Fig. 6). This approach allows the measurement of relative distances between two loci within the same nucleus, providing more control for reducing inter-cellular variation.

In addition to two-dimensional distances from gene loci to nuclear periphery, the next steps would also include three-dimensional distance measurement from loci to interior heterochromatin. The expected outcome is that the *Spi1* gene loci would be positioned further away from the repressed heterochromatic region than *Gata1*.

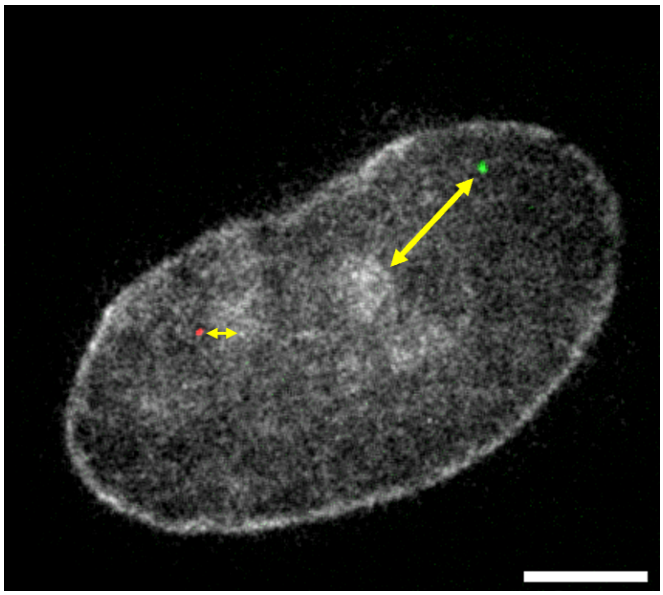

Figure 6. Example of dual-channel DNA FISH image, stained with Hoechst 33258. Green is *spi1*, and red is *gata1*. Distances from gene loci to interior heterochromatin are measured as indicated by the yellow lines with arrows in 3D. Scale bar: 2 μm.

2.4.2 SCEPTRE

Preliminary SCEPTRE images were acquired to assess the feasibility of simultaneously visualizing the gene loci of interest and histone modifications (H3K4me3 and H3K27me3) in expanded BMDMs.

The next steps would include quantitative analysis of these signals, including the classification of individual alleles as active, repressive, or bivalent based on H3K4me3 and H3K27me3 intensity profiles.

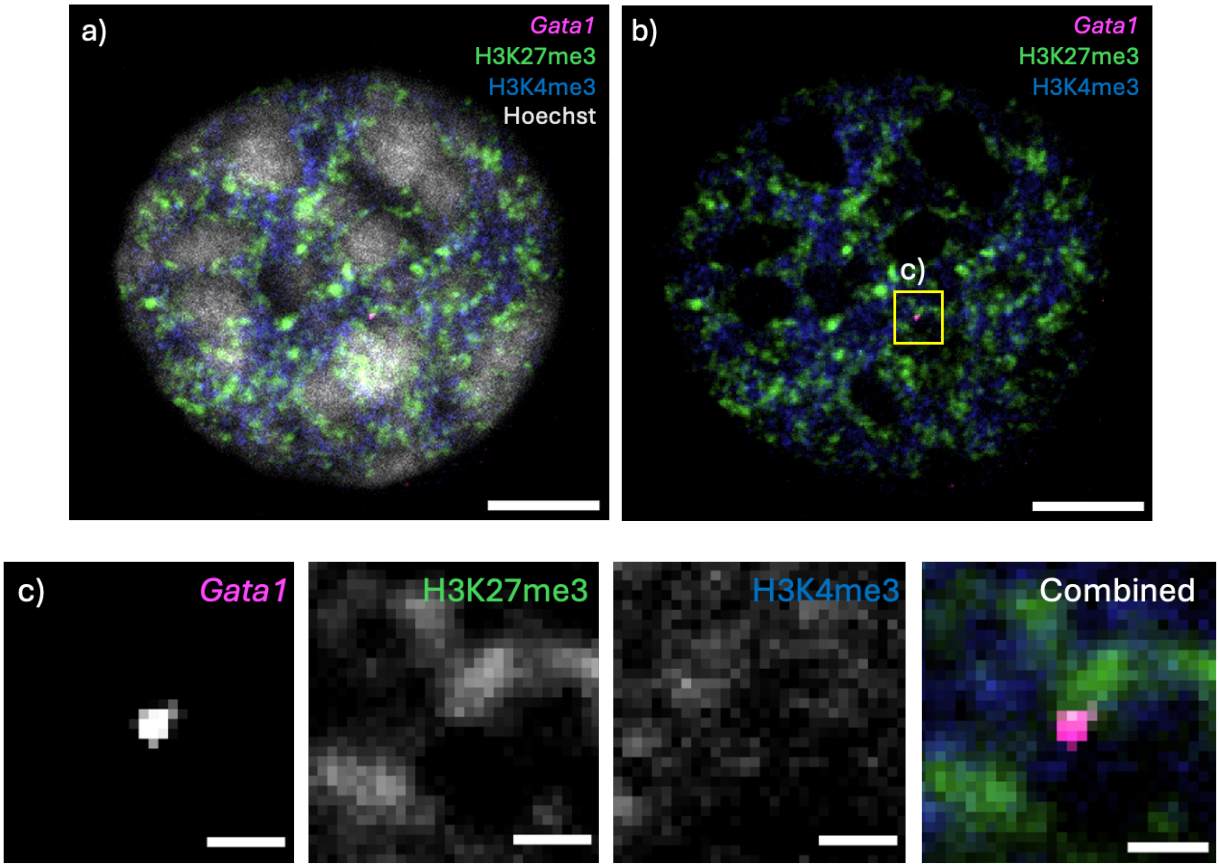

Figure 7. Example image of SCEPTRE that distinguishes H3K4me3 v H3K27me3 at the gata1 gene loci. a) An expanded BMDM with immunolabeled H3K27me3 (green) and H3K4me3 (blue) marks, FISH-labeled *Gata1* (magenta), and Hoechst 33258 in gray. b) The same image as a) without Hoechst staining for better visualization of immunolabels and FISH labels. c) Zoomed in view of the approximate center plane of the labeled *Gata1* locus in b). Scale bar: a, b) 2µm, c) 200 nm.

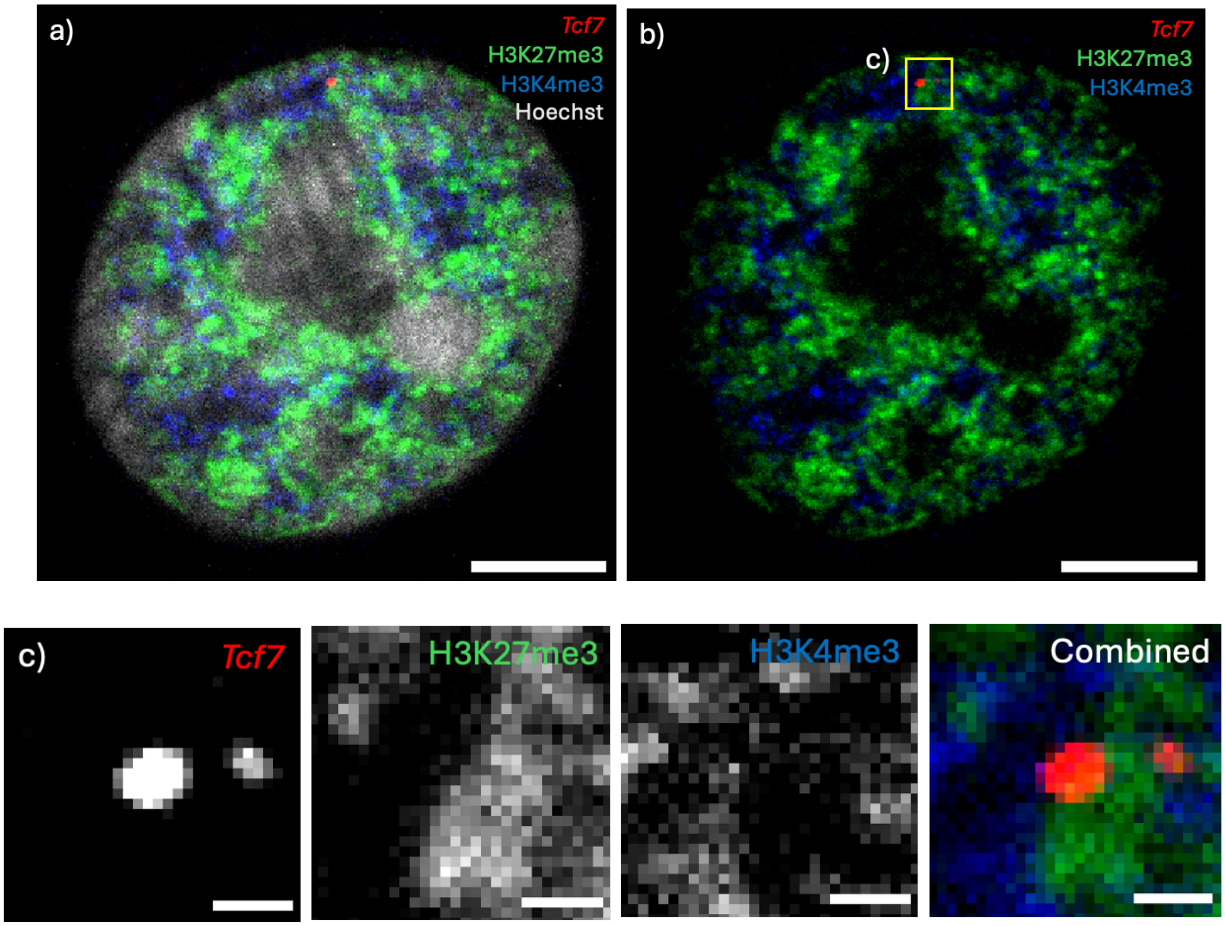

Figure 8. Example image of SCEPTRE that distinguishes H3K4me3 v H3K27me3 at the tcf7 gene loci. a) An expanded BMDM with immunolabeled H3K27me3 (green) and H3K4me3 (blue) marks, FISH-labeled *Tcf7* (red), and Hoechst 33258 in gray. b) The same image as a) without Hoechst staining for better visualization of immunolabels and FISH labels. c) Zoomed in view of the approximate center plane of the labeled *Tcf7* loci in b). Scale bar: a, b) 2μm, c) 200 nm.

2.5 Conclusions

In conclusion, both ExM and DNA FISH introduce minimal distortion to the murine BMDMs and are robust methods for studying the spatial distribution of lineage-defining gene

loci, relative to the nuclear periphery and to the chromatin structures. The preliminary work was established for dual-channel DNA FISH and for SCEPTRE, targeting *Spi1*, *Gata1*, and *Tcf7*, and future can build upon current data to provide more quantitative analyses on the distribution of the histone marks in relation to these lineage-defining genes in hematopoiesis.

2.6 Methods and Reagents

2.6.1 Reagents

Reagents for expansion hydrogel polymerization and digestion: 40% (w/v) acrylamide (AA; Bio-Rad Laboratories, cat. no. 161-0140), 2% (w/v) bis-acrylamide (BA; Bio-Rad Laboratories, cat. no. 161-0142), Sodium acrylate (SA; Sigma-Aldrich, cat. no. 408220), Tetramethylethylenediamine (TEMED, Bio-Rad, cat. no. 1610800), Ammonium persulfate (APS, Bio-Rad, cat. no.1610700), Sodium dodecyl sulfate (SDS; Sigma-Aldrich, cat. no. L3771), Sodium chloride (NaCl; Fisher Scientific, cat. no. 271). Proteinase K (Thermo Scientific, cat.no. EO0491), Tris-Acetate-EDTA Buffer (TAE, Invitrogen, 15558-042), Phosphate Buffer Saline (PBS, Gibco, 70011-044), Methacrylic acid N-hydroxysuccinimide (MA-NHS, Sigma-Aldrich, 730300), Triton-X -100 (TX-100, Sigma Aldrich, cat. no.61-2754)

Reagents for immunostaining: 32% paraformaldehyde aqueous solution (PFA, Electron Microscopy Sciences, RT15714), Glycine (Bio-Rad, 161-0718), Bovine serum albumin (BSA; Rockland Immunochemicals Inc, item no. BAS-50), Sodium Azide Granular (NaN3, Fisher Scientific, cat no. S2271)

Reagents for cell culture: Ham's F-12 Nutrient Mix liquid medium (1×; Gibco, cat. no. 11765-054, HEPES (1 M; Gibco, cat. no. 15630-080) Penicillin–streptomycin–glutamine (PSG, 100×; Gibco, cat. no. 10378-016) Insulin–transferrin–selenium–ethanolamine (ITSX; 100×; Gibco, cat.

no. 51500-056), Polyvinyl alcohol (PVA; 87–90%-hydrolyzed; Sigma-alrich, cat. no. P8136), Dulbecco's Modified Eagle Medium (DMEM, Gibco, cat.no. 11995065), Penicillin-Streptomycin (10,000 U/mL) (Pen-Strep, Gibco, cat. no. 15140122), Fetal Bovine Serum (FBS, Gibco, 26140079), Recombinant murine stem cell colony factor (SCF, Peprotech, cat. no. 250-03), Recombinant murine thrombopoietin (TPO, Peprotech, cat. no.315-14), Recombinant murine granulocyte-macrophage colony stimulating factor (GM-CSF, Peprotech, cat. no. 315-03), Hanks balanced salt solution (HBSS, Thermo Fisher Scientific, cat. No. 14025076)

Reagents for primary conjugation: Sodium Bicarbonate ($NaHCO_3$, Fisher Scientific, S233), Sodium Hydroxide (Fisher Scientific, S399), Alexa Fluor 488 NHS ester (Lumiphore, cat. No. 11820)

2.6.2 Isolation of bone marrow for primary cells

8-week-old C57/BL6 male mice were obtained and euthanized with carbon dioxide for 5 minutes before cervical dislocation was performed. Mouse femora and tibiae were harvested for downstream culture of hematopoietic stem cells and bone-marrow-derived macrophages. All protocols and methods involving animals in this work were approved by the Institutional Animal Care and Use Committee at the University of Washington.

2.6.3 Cell culture of bone marrow derived macrophages (BMDMs)

Muscle tissue was removed from mouse femora and tibiae using a razor blade, before cleaned thoroughly with 70% ethanol. Each bone was flushed with 3 mL of HBH solution (0.5% (w/v) BSA, 10 mM HEPES in HBSS) using a 23-gauge needle. Bone marrow suspension was filtered through a 70-micron filter to remove bone chunks. The solution was centrifuged, and the

supernatant was removed. 5 mL of freshly made 1x red blood cell lysis buffer (149 mM NH_4Cl, 10mM $NaHCO_3$, 1mM EDTA in water) was added, and the solution was incubated for 5 min at room temperature. Then 10 mL of macrophage media (10% heat inactivated FBS and 1x Penicillin-Streptomycin in high glucose DMEM) was added to the solution and centrifuged for 5 minutes. The supernatant was removed before another 5 mL of macrophage media was added. The bone marrow cell solution was filtered through a 70 um filter. The cells were plated in a 24-well or an 8-well chamber slide with a concentration of approximately 1e6 cells/well and spiked with GM-CSF (10 ng/mL). The media was changed on day 3, and the cells were fixed with 4% PFA for 10 minutes.

2.6.4 Preparation for primary antibody conjugation

The conjugation was performed in an eppendorf tube by mixing 40 uL of D x Hu antibody, 10 uL of pH (~9.45) adjusted 1M $NaHCO_3$, and 2-5 ug of NHS ester functionalized fluorophore. The reaction was left to react for 10 minutes, kept away from ambient light. A NAP5 column (GE Healthcare Life Sciences, 17085301) was obtained, and the reaction mixture was added to the column for purification. The purified sample was collected and characterized using ultraviolet/visible adsorption spectroscopy and immunostaining controls.

2.6.5 Immunostaining

Fixed BMDMs were incubated in block/perm (B/P) solution (3% (w/v) BSA, 0.5% (v/v) Triton-X) at room temp for 60 minutes, then incubated in a primary antibody diluted in B/P for 1 hour at room temp, before solution was removed and washed 3 times with B/P. Then the cells were incubated in a secondary antibody diluted in B/P for 1 hour at room temperature. The solution

was removed before the cells were washed 3 times with B/P. Lastly, the cells were incubated in 1:1000 Hoechst 33258 diluted in 1x PBS for 10 minutes at room temperature. Then the cells were washed with 1x PBS 3 times.

2.6.6 Gelation and expansion

Fixed BMDMs were treated with 5 mM MA-NHS for 20 minutes at room temperature, then washed with excess 1x PBS. The cells were then incubated with a pre-warmed (37ºC) ExM monomer solution (10% (v/v) 1x PBS, 2M NaCl, 8.525% (w/v) sodium acrylate, 2.5% (w/v) acrylamide, 0.15% (w/v) bis-acrylamide in DI water) for 15 minutes at room temperature. 1.5 µl of 10% TEMED, and 1.5 µl of 10% ammonium persulfate (APS) were added to 97 µl of the pre-warmed (37ºC) ExM monomer solution in an Eppendorf tube. Immediately after adding APS, the solution was mixed quickly, then 60 µl of the gelation solution was pipetted onto a square coverslip, placed inside a lunchbox. The 12 mm cover glass was placed onto the gelation solution, with the cell side facing down. Nitrogen gas was pumped into the lunch box, which was then incubated at 37 ºC for 1 hour. After the incubation, the gel was carefully peeled off from the cover glass. The gel was transferred into a 12-well plate, containing 2 mL of freshly prepared digestion buffer (1x TAE buffer, 0.8 M guanidine-HCl, 0.5% Triton X-100) along with 2 uL of Hoechst 33258 and 20 uL of protein kinase. The gel was incubated overnight at 37 ºC. The gel was expanded in 3 exchanges of DI water for 30 minutes each on the second day.

2.6.7 DNA FISH

The DNA FISH probes were designed using OligoMiner by another lab member, Dr. Madeline Wong, in the Vaughan Group.

A gelled and fully expanded sample was cut into approximate dimensions of 5 mm by 10 mm. The sample was first incubated in 2x SCCT at room temperature for 10 minutes, then in hybridization buffer (50% (v/v) 4x SCCT and 50% (v/v) formamide) at room temperature for 10 minutes. Then the sample was incubated in a new hybridization buffer at 60 C for 30 minutes. Then the sample was incubated in DNA FISH solution (10% (v/v) 20x SCC, 50% (v/v) formamide, 20% dextran sulfate, 1% sodium azide, with a final DNA probe concentration of 600 nM for spi1, and 1200 nM for gata1 and tcf7) at 95 °C for 5 minutes. Then the sample was incubated in the same DNA FISH solution at 42 °C overnight. The sample was washed the second day with 2x SCCT at 60 °C, and then 37 °C, for 15 minutes each. The sample was re-stained with Hoechst 33258 (1 ug/mL) or SYBR GREEN I (1x) for 10 minutes at room temperature, before it was washed with 2x SCCT at room temperature. The sample was expanded in DI water for at least 15 minutes before imaging.

2.6.8 Image acquisition

Gelled and expanded samples of size ~0.5 mm x 0.5 mm were adhered to a poly-L-lysine-coated rectangular no. 1.5 coverslip or an 8-well chamber slide. For samples imaged pre-expansion and pre-gelation, the cells were cultured and fixed directly in 8-well chamber slides and imaged while they were still inside the slides. All samples were imaged with a homebuilt spinning disk confocal microscope using a Nikon CFI60 Plan Apochromat 60x 1.27 NA water-immersion objective.

2.6.9 Distortion analysis and *Elastix*

The open-source software *Elastix* was used for rigid (similarity, or euler) and non-rigid (B-spline) registration of pre-and post-expansion or pre-and-post DNA FISH images. *Elastix* was controlled through Command Prompt. The typical command line is as follows: *elastix -f fixed.mhd -m moving.mhd -p Parameters.txt -out* ., where the fixed image is the pre-expansion or pre-DNA-FISH image, the moving image is the post-expansion or post-DNA-FISH image, and the parameters file contains the parameters and type of transformation (rigid or non-rigid) used for the registration. The registration was typically a two-step process, where a rigid transformation was performed first, before the resulting image from the rigid transformation was used as the fixed image for a non-rigid transformation. After the non-rigid transformation, the deformation information was stored in an automatically generated file called "TransformParameters.0.txt," which was used for generating an RMS error plot. For pre-post expansion registration, the pre-expansion image was first manually adjusted (i.e., rotation, expansion, and intensity adjusted) to better fit the post-expansion image, which was also manually adjusted (i.e., gaussian blur). For pre-post-DNA-FISH, only the intensity of the pre-DNA-FISH image was manually dimmed so it better matched the post image.

2.7 References

(1) Martin, E. W.; Rodriguez y Baena, A.; Reggiardo, R. E.; Worthington, A. K.; Mattingly, C. S.; Poscablo, D. M.; Krietsch, J.; McManus, M. T.; Carpenter, S.; Kim, D. H.; Forsberg, E. C. Dynamics of Chromatin Accessibility During Hematopoietic Stem Cell Differentiation Into Progressively Lineage-Committed Progeny. *Stem Cells* **2023**, *41* (5), 520–539. https://doi.org/10.1093/stmcls/sxad022.

(2) 3 Ontogeny of Hematopoiesis: Examining the Emergence of Hematopoietic Cells in the Vertebrate Embryo. **2003**, *53*, 139–158. https://doi.org/10.1016/S0070-2153(03)53004-6.

(3) Johnson, J. L.; Georgakilas, G.; Petrovic, J.; Kurachi, M.; Cai, S.; Harly, C.; Pear, W. S.; Bhandoola, A.; Wherry, E. J.; Vahedi, G. Lineage-Determining Transcription Factor TCF-1 Initiates the Epigenetic Identity of T Cells. *Immunity* **2018**, *48* (2), 243-257.e10. https://doi.org/10.1016/j.immuni.2018.01.012.

(4) Lucas, D. Structural Organization of the Bone Marrow and Its Role in Hematopoiesis. *Curr. Opin. Hematol.* **2021**, *28* (1), 36–42. https://doi.org/10.1097/MOH.0000000000000621.

(5) Pinho, S.; Frenette, P. S. Haematopoietic Stem Cell Activity and Interactions with the Niche. *Nat. Rev. Mol. Cell Biol.* **2019**, *20* (5), 303–320. https://doi.org/10.1038/s41580-019-0103-9.

(6) Pucella, J. N.; Upadhaya, S.; Reizis, B. The Source and Dynamics of Adult Hematopoiesis: Insights from Lineage Tracing. *Annu. Rev. Cell Dev. Biol.* **2020**, *36* (Volume 36, 2020), 529–550. https://doi.org/10.1146/annurev-cellbio-020520-114601.

(7) Jagannathan-Bogdan, M.; Zon, L. I. Hematopoiesis. *Development* **2013**, *140* (12), 2463–2467. https://doi.org/10.1242/dev.083147.

(8) Loughran, S. J.; Kruse, E. A.; Hacking, D. F.; de Graaf, C. A.; Hyland, C. D.; Willson, T. A.; Henley, K. J.; Ellis, S.; Voss, A. K.; Metcalf, D.; Hilton, D. J.; Alexander, W. S.; Kile, B. T. The Transcription Factor Erg Is Essential for Definitive Hematopoiesis and the Function of Adult Hematopoietic Stem Cells. *Nat. Immunol.* **2008**, *9* (7), 810–819. https://doi.org/10.1038/ni.1617.

(9) Nombela-Arrieta, C.; Manz, M. G. Quantification and Three-Dimensional Microanatomical Organization of the Bone Marrow. *Blood Adv.* **2017**, *1* (6), 407–416. https://doi.org/10.1182/bloodadvances.2016003194.

(10) Sheu, T.-T.; Chiang, B.-L. Lymphopenia, Lymphopenia-Induced Proliferation, and Autoimmunity. *Int. J. Mol. Sci.* **2021**, *22* (8), 4152. https://doi.org/10.3390/ijms22084152.

(11) Gomes, A. C.; Gomes, M. S. Hematopoietic Niches, Erythropoiesis and Anemia of Chronic Infection. *Exp. Hematol.* **2016**, *44* (2), 85–91. https://doi.org/10.1016/j.exphem.2015.11.007.

(12) Positive Feedback Between PU.1 and the Cell Cycle Controls Myeloid Differentiation. *Science*.

(13) Burda, P.; Laslo, P.; Stopka, T. The Role of PU.1 and GATA-1 Transcription Factors during Normal and Leukemogenic Hematopoiesis. *Leukemia* **2010**, *24* (7), 1249–1257. https://doi.org/10.1038/leu.2010.104.

(14) Lizana, L.; Schwartz, Y. B. The Scales, Mechanisms, and Dynamics of the Genome Architecture. *Sci. Adv. 10* (15), eadm8167. https://doi.org/10.1126/sciadv.adm8167.

(15) Allis, C. D.; Jenuwein, T. The Molecular Hallmarks of Epigenetic Control. *Nat. Rev. Genet.* **2016**, *17* (8), 487–500. https://doi.org/10.1038/nrg.2016.59.

(16) Arents, G.; Burlingame, R. W.; Wang, B. C.; Love, W. E.; Moudrianakis, E. N. The Nucleosomal Core Histone Octamer at 3.1 A Resolution: A Tripartite Protein Assembly and a Left-Handed Superhelix. *Proc. Natl. Acad. Sci.* **1991**, *88* (22), 10148–10152. https://doi.org/10.1073/pnas.88.22.10148.

(17) Misteli, T. The Self-Organizing Genome: Principles of Genome Architecture and Function. *Cell* **2020**, *183* (1), 28–45. https://doi.org/10.1016/j.cell.2020.09.014.

(18) Herman, A. B.; Tsitsipatis, D.; Gorospe, M. Integrated lncRNA Function upon Genomic and Epigenomic Regulation. *Mol. Cell* **2022**, *82* (12), 2252–2266. https://doi.org/10.1016/j.molcel.2022.05.027.

(19) Chinwalla, A. T.; Initial Sequencing and Comparative Analysis of the Mouse Genome. *Nature* **2002**, *420* (6915), 520–562. https://doi.org/10.1038/nature01262.

(20) Andersson, R.; Sandelin, A.; Danko, C. G. A Unified Architecture of Transcriptional Regulatory Elements. *Trends Genet.* **2015**, *31* (8), 426–433. https://doi.org/10.1016/j.tig.2015.05.007.

(21) Youssef, N.; Budd, A.; Bielawski, J. P. Introduction to Genome Biology and Diversity. In *Evolutionary Genomics: Statistical and Computational Methods*; Anisimova, M., Ed.; Springer: New York, NY, 2019; pp 3–31. https://doi.org/10.1007/978-1-4939-9074-0_1.

(22) Kouzarides, T. Chromatin Modifications and Their Function. *Cell* **2007**, *128* (4), 693–705. https://doi.org/10.1016/j.cell.2007.02.005.

(23) Bannister, A. J.; Kouzarides, T. Regulation of Chromatin by Histone Modifications. *Cell Res.* **2011**, *21* (3), 381–395. https://doi.org/10.1038/cr.2011.22.

(24) Saksouk, N.; Simboeck, E.; Déjardin, J. Constitutive Heterochromatin Formation and Transcription in Mammals. *Epigenetics Chromatin* **2015**, *8* (1), 3. https://doi.org/10.1186/1756-8935-8-3.

(25) Grewal, S. I. S. The Molecular Basis of Heterochromatin Assembly and Epigenetic Inheritance. *Mol. Cell* **2023**, *83* (11), 1767–1785. https://doi.org/10.1016/j.molcel.2023.04.020.

(26) Rodrigues, C. P.; Shvedunova, M.; Akhtar, A. Epigenetic Regulators as the Gatekeepers of Hematopoiesis. *Trends Genet.* **2021**, *37* (2), 125–142. https://doi.org/10.1016/j.tig.2020.09.015.

(27) Farsetti, A.; Illi, B.; Gaetano, C. How Epigenetics Impacts on Human Diseases. *Eur. J. Intern. Med.* **2023**, *114*, 15–22. https://doi.org/10.1016/j.ejim.2023.05.036.

(28) Condemi, L.; Mocavini, I.; Aranda, S.; Di Croce, L. Polycomb Function in Early Mouse Development. *Cell Death Differ.* **2025**, *32* (1), 90–99. https://doi.org/10.1038/s41418-024-01340-3.

(29) Sun, H.; Wang, Y.; Wang, Y.; Ji, F.; Wang, A.; Yang, M.; He, X.; Li, L. Bivalent Regulation and Related Mechanisms of H3K4/27/9me3 in Stem Cells. *Stem Cell Rev. Rep.* **2022**, *18* (1), 165–178. https://doi.org/10.1007/s12015-021-10234-7.

(30) Cedar, H.; Bergman, Y. Epigenetics of Haematopoietic Cell Development. *Nat. Rev. Immunol.* **2011**, *11* (7), 478–488. https://doi.org/10.1038/nri2991.

(31) Rothenberg, E. V.; Hosokawa, H.; Ungerbäck, J. Mechanisms of Action of Hematopoietic Transcription Factor PU.1 in Initiation of T-Cell Development. *Front. Immunol.* **2019**, *10*. https://doi.org/10.3389/fimmu.2019.00228.

(32) Minderjahn, J.; Schmidt, A.; Fuchs, A.; Schill, R.; Raithel, J.; Babina, M.; Schmidl, C.; Gebhard, C.; Schmidhofer, S.; Mendes, K.; Ratermann, A.; Glatz, D.; Nützel, M.; Edinger, M.; Hoffmann, P.; Spang, R.; Längst, G.; Imhof, A.; Rehli, M. Mechanisms Governing the

Pioneering and Redistribution Capabilities of the Non-Classical Pioneer PU.1. *Nat. Commun.* **2020**, *11* (1), 402. https://doi.org/10.1038/s41467-019-13960-2.

(33) Kueh, H. Y.; Champhekar, A.; Nutt, S. L.; Elowitz, M. B.; Rothenberg, E. V. Positive Feedback Between PU.1 and the Cell Cycle Controls Myeloid Differentiation. *Science* **2013**, *341* (6146), 670–673. https://doi.org/10.1126/science.1240831.

(34) Cantor, A. B.; Katz, S. G.; Orkin, S. H. Distinct Domains of the GATA-1 Cofactor FOG-1 Differentially Influence Erythroid versus Megakaryocytic Maturation. *Mol. Cell. Biol.* **2002**, *22* (12), 4268–4279. https://doi.org/10.1128/MCB.22.12.4268-4279.2002.

(35) Tsang, A. P.; Fujiwara, Y.; Hom, D. B.; Orkin, S. H. Failure of Megakaryopoiesis and Arrested Erythropoiesis in Mice Lacking the GATA-1 Transcriptional Cofactor FOG. *Genes Dev.* **1998**, *12* (8), 1176–1188.

(36) Gao, J.; Chen, Y.-H.; Peterson, L. C. GATA Family Transcriptional Factors: Emerging Suspects in Hematologic Disorders. *Exp. Hematol. Oncol.* **2015**, *4* (1), 28. https://doi.org/10.1186/s40164-015-0024-z.

(37) Escobar, G.; Mangani, D.; Anderson, A. C. T Cell Factor 1: A Master Regulator of the T Cell Response in Disease. *Sci. Immunol.* **2020**, *5* (53), eabb9726. https://doi.org/10.1126/sciimmunol.abb9726.

(38) Xing, S.; Li, F.; Zeng, Z.; Zhao, Y.; Yu, S.; Shan, Q.; Li, Y.; Phillips, F. C.; Maina, P. K.; Qi, H. H.; Liu, C.; Zhu, J.; Pope, R. M.; Musselman, C. A.; Zeng, C.; Peng, W.; Xue, H.-H. Tcf1 and Lef1 Transcription Factors Establish CD8+ T Cell Identity through Intrinsic HDAC Activity. *Nat. Immunol.* **2016**, *17* (6), 695–703. https://doi.org/10.1038/ni.3456.

(39) Zhao, X.; Shan, Q.; Xue, H.-H. TCF1 in T Cell Immunity: A Broadened Frontier. *Nat. Rev. Immunol.* **2022**, *22* (3), 147–157. https://doi.org/10.1038/s41577-021-00563-6.

(40) Grandi, F. C.; Modi, H.; Kampman, L.; Corces, M. R. Chromatin Accessibility Profiling by ATAC-Seq. *Nat. Protoc.* **2022**, *17* (6), 1518–1552. https://doi.org/10.1038/s41596-022-00692-9.

(41) Chen, A.; Chen, D.; Chen, Y. Advances of DNase-Seq for Mapping Active Gene Regulatory Elements across the Genome in Animals. *Gene* **2018**, *667*, 83–94. https://doi.org/10.1016/j.gene.2018.05.033.

(42) Park, P. J. ChIP–Seq: Advantages and Challenges of a Maturing Technology. *Nat. Rev. Genet.* **2009**, *10* (10), 669–680. https://doi.org/10.1038/nrg2641.

(43) Meers, M. P.; Bryson, T. D.; Henikoff, J. G.; Henikoff, S. Improved CUT&RUN Chromatin Profiling Tools. *eLife* **2019**, *8*, e46314. https://doi.org/10.7554/eLife.46314.

(44) Woodworth, M. A.; Ng, K. K. H.; Halpern, A. R.; Pease, N. A.; Nguyen, P. H. B.; Kueh, H. Y.; Vaughan, J. C. Multiplexed Single-Cell Profiling of Chromatin States at Genomic Loci by Expansion Microscopy. *Nucleic Acids Res.* **2021**, *49* (14), e82. https://doi.org/10.1093/nar/gkab423.

(45) Chen, F.; Tillberg, P. W.; Boyden, E. S. Expansion Microscopy. *Science* **2015**, *347* (6221), 543–548. https://doi.org/10.1126/science.1260088.

(46) Bucevičius, J.; Lukinavičius, G.; Gerasimaitė, R. The Use of Hoechst Dyes for DNA Staining and Beyond. *Chemosensors* **2018**, *6* (2), 18. https://doi.org/10.3390/chemosensors6020018.

(47) Wassie, A. T.; Zhao, Y.; Boyden, E. S. Expansion Microscopy: Principles and Uses in Biological Research. *Nat. Methods* **2019**, *16* (1), 33–41. https://doi.org/10.1038/s41592-018-0219-4.

(48) Vanheusden, M.; Vitale, R.; Camacho, R.; Janssen, K. P. F.; Acke, A.; Rocha, S.; Hofkens, J. Fluorescence Photobleaching as an Intrinsic Tool to Quantify the 3D Expansion Factor of Biological Samples in Expansion Microscopy. *ACS Omega* **2020**, *5* (12), 6792–6799. https://doi.org/10.1021/acsomega.0c00118.